RSC Advances

PAPER

View Article Online
View Journal | View Issue

Cite this: *RSC Adv.*, 2023, **13**, 27147

Hierarchical dandelion-like CoS_2 hollow microspheres: self-assembly and controllable microwave absorption performance†

Dongwei Xu, *[a] Feifan Zhang,[a] Huanhuan Guo,[a] Sitong Liu,[a] Shuaijiang Ma,[b] Xiaoqin Guo*[a] and Ping Chen *[c]

The emerging electromagnetic radiation and interference problems have promoted the rapid development of microwave absorption materials (MAMs). However, it remains a severe challenge to construct high-performance microwave absorption materials with broadband, lightweight and corrosion resistance within low filling contents. Herein, hierarchical dandelion-like CoS_2 hollow microspheres were reasonably constructed *via* a solvothermal-hydrothermal etching-*in situ* vulcanization process. The structure morphology, composition and electromagnetic performance of all samples have been thoroughly tested. The research results demonstrated that the structure morphology of the prepared samples with a volume ratio of 1 : 1 between ethanol and H_2O remained intact without serious damage. Notably, the as-obtained hierarchical dandelion-like CoS_2 hollow microspheres (25 wt%) exhibited excellent microwave absorption capacity with a minimum reflection loss (RLmin) of −47.3 dB and the corresponding effective absorption bandwidth (EAB) of 8.4 GHz at 3.3 mm. Moreover, the broadest effective absorption bandwidth (EAB, RL < −10 dB) reached 9.0 GHz (9.0–18.0 GHz) at the matching thickness of 3.2 mm. The unparalleled multiple features including hierarchical hollow structure, tunable complex permittivity as well as the enhanced impedance matching endowed CoS_2 great promise as high-performance microwave absorbers for solving the problem of electromagnetic pollution.

Received 20th July 2023
Accepted 23rd August 2023

DOI: 10.1039/d3ra04890j

rsc.li/rsc-advances

Introduction

With the rapid upgrading of electronic instruments, electromagnetic radiation and interference have undoubtedly become prominent, which seriously affect the normal operation of electronic equipment and the information safety as well as human health.[1–3] Electromagnetic absorbing materials (EAMs), which can convert electromagnetic energy to thermal energy, are essential to effectively prevent the leakage of electromagnetic information and suppress the radiation and interference of electromagnetic waves.[4–6]

In order to obtain excellent electromagnetic wave absorption properties, the microstructure design and composition modification of composite materials are very important. Many studies have confirmed that the microwave absorption performance (MAP) depends mainly on the electromagnetic parameters (including complex permittivity and complex permeability) and impedance-matching properties, which are closely related to the microstructures, components, and geometry of the absorbing materials.[7,8] Compared to conventional absorbents, various nanomaterials with diverse morphologies and structures such as nanowires,[9] nanoflakes,[10] and nanospheres[11] always exhibit moderate microwave absorption performance. Therefore, tremendous research efforts have been devoted to designing and developing advanced and efficient absorbing materials. Moreover, texture regulation shed new lights on the design, synthesis, and performance regulation of absorbents. As expected, porous micro/nanostructures with hollow configurations in view of their unique structural features including well-defined interior voids, low density as well as large surface area can expose more active surfaces and enhance charge transfer efficiency, resulting in improved electromagnetic performance.[12,13] Wu *et al.* adopted the co-modification strategies of poly-dopamine coating and wet impregnation to construct CoS_2 magnetic double-shell microspheres for achieving the optimized microwave absorption performance.[14] Chen *et al.* successfully prepared the nitrogen-doped porous carbon decorated with core–shell Ni_3Sn_2@carbon particles through a simple salt-template pyrolysis approach. Due to the intriguing 3D porous and core–shell structure, rich heterogeneous interface as well as perfect conductive network, the

[a]School of Material Science and Engineering, Henan Key Laboratory of Aeronautical Materials and Application Technology, Zhengzhou University of Aeronautics, Zhengzhou, Henan 450046, China. E-mail: xudongwei1029@126.com

[b]Faculty of Engineering, Huanghe Science & Technology University, Zhengzhou 450063, China

[c]State Key Laboratory of Fine Chemicals, Dalian University of Technology, Dalian, 116024, China. E-mail: chenping_898@126.com

† Electronic supplementary information (ESI) available. See DOI: https://doi.org/10.1039/d3ra04890j

obtained composites possessed the RLmin of −54.01 dB and wide EAB of 7.36 GHz under a low filling contents.[15]

Recently, transition metal sulfides (TMSs) because of their remarkable advantages such as outstanding electronic properties, thermal stability and high resistance to oxidation and corrosion have been extensive investigated and been widely used in the field of energy storage devices,[16] electrochemical hydrogen evolution,[17] photocatalysis[18] and so on. As a kind of complicated transition metal dichalcogenide, cobalt disulphide (CoS_2) with inherent chemical and structural stability as well as the unique magnetic-electrical properties have been used in supercapacitors, lithium-ion batteries, and spintronic devices, which in turn confirmed CoS_2 can be a candidate for microwave absorption due to its dielectric loss capability and part of the magnetic loss. Inspired by the structural point of view, CoS_2 with different morphologies showed various structural advantages and performance characteristics in the field of microwave absorption. In particular, CoS_2 with hierarchical and hollow structure possess lightweight feature. Furthermore, the hollow structure is conducive to the enhanced impedance matching characteristics and providing large hollow interfaces as well as generating multiple reflections as much as possible to extend the transmission path, all of them are favorable for microwave absorption enhancement.

In this work, hierarchical dandelion-like CoS_2 hollow microspheres were synthesized using cobalt glycerate (CoG) solid microspheres as precursors followed by solvothermal-hydrothermal etching and *in situ* vulcanization process. When the volume ratio of ethanol to water was set as 1 : 1, the hierarchical dandelion-like morphology of Co-based carbonate hydroxide microspheres could be obtained, and the hollow structure has almost no change after *in situ* vulcanization. The effect of structural on the absorption properties of CoS_2 hollow microspheres was investigated in depth. Due to the unique hierarchical hollow structure and the optimized impedance matching, when the filling is 25 wt%, the RLmin of CoS_2 samples at 3.3 mm is −47.3 dB and the maximum EAB at 3.2 mm is 9.0 GHz, which made the composites a promising class of microwave absorption materials for a lightweight and wide range of applications.

Materials

All chemicals were at analytic reagent grade and used as received. Cobalt nitrate ($Co(NO_3)_2 \cdot 6H_2O$) and thioacetamide (TAA) were purchased from Sinopharm Chemical Reagent Co., Ltd (Shanghai, China). Anhydrous ethanol, glycerol and isopropanol were purchased from Aladdin Corporation.

Synthesis of Co-glycerate precursor solid microspheres

In the typical synthesis process, $Co(NO_3)_2 \cdot 6H_2O$ (3.0 mmol) was dissolved into 70 mL glycerol-isopropanol mixed solvent ($V_g : V_i = 1 : 6$) under ultrasonic stirring to obtain clear solution. After that, the clear solution was sealed into 100 mL stainless steel autoclave and maintained at 200 °C for 12 h. Then, the autoclave was cooled down to room temperature naturally, the products were washed with ethanol several times. Finally, the Co-glycerate precursor solid microspheres were separated and purified by centrifugation and drying.

Synthesis of hierarchical Co_3O_4 hollow microspheres

The Co-glycerate precursor solid microspheres (0.1 g) were dispersed in 60 mL ethanol/H_2O mixed solvent (The volume ratio is set to 2 : 1, 1 : 1, 1 : 2) by ultrasonic treatment for 30 min, subsequently the mixed suspension was sealed into 100 mL stainless steel autoclave and kept at 160 °C for 8 h. The as-obtained products were collected and washed with deionized water and ethanol successively.

Synthesis of dandelion-like CoS_2 hollow microspheres

Firstly, 0.1 g hierarchical Co_3O_4 hollow microspheres were dispersed into ethanol solvent containing TAA with ultrasonic treatment for 15 min to form homogeneous suspension. Then, the suspension was poured into the 100 mL teflon lined autoclave and reacted at 140 °C for 6 h for *in situ* vulcanization reaction. Finally, the resulting products were collected and washed with deionized water and ethanol successively to obtain dandelion-like CoS_2 hollow microspheres.

Characterization

The crystal structures and phase compositions were investigated by X-ray powder diffractometer using Cu Kα radiation (XRD, SmartLabX, λ = 0.15418 nm). The morphology and microstructure of samples were characterized on field-emission scanning electron microscope (FESEM, Germany) and transmission electron microscope (TEM, Tecnai F30, USA). Surface elemental analysis were characterized by X-ray photoelectron spectra (XPS) using ultrahigh vacuum apparatus built by ESCALAB 250 (USA). Nitrogen adsorption isotherm measurements were performed with a Quanta 4200e surface area analyzer.

To investigate the electromagnetic wave absorption properties, different proportions coaxial ring test samples of obtained dandelion-like CoS_2 hollow microspheres with paraffin matrix (Φ_{outer} = 7 mm and Φ_{inner} = 3 mm, where the symbol Φ represents the diameter) were measured for electromagnetic parameters over the 1–18 GHz range. Different samples named as CS15, CS25 and CS35 were prepared by mixing powders (15 wt%, 25 wt%, 35 wt%) with paraffin followed by compressing into coaxial rings, respectively.

Results and discussion

The 3D hierarchical dandelion-like CoS_2 hollow microspheres was prepared by a combination of solvothermal-hydrothermal etching-in situ vulcanization, as schematically illustrated in Fig. 1. In the initial step, Co^{2+} reacted with glycerol at 200 °C for 12 h to get Co-glycerate solid microspheres (Co-GSMs). Subsequently, the hierarchical Co_3O_4 hollow microspheres were obtained through hydrothermal etching process in ethanol/H_2O mixed solvent. Finally, the hierarchical CoS_2 hollow

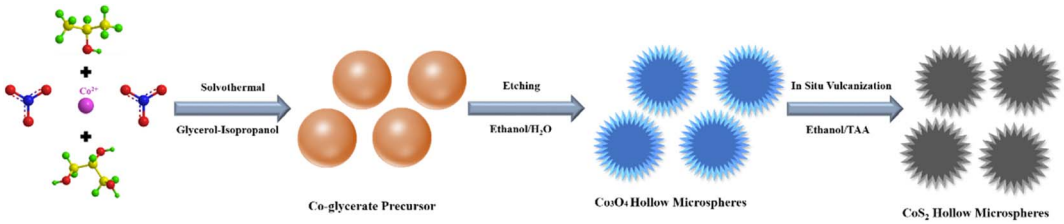

Fig. 1 Schematic illustration of the formation process for hierarchical dandelion-like CoS_2 hollow microspheres.

microspheres were obtained by *in situ* vulcanization under hydrothermal conditions.

The representative morphology and microstructures detail of Co-GSMs, Co_3O_4 and hierarchical CoS_2 hollow microspheres were elucidated by scanning electron microscopy (SEM) and transmission electron microscopy (TEM). As depicted in Fig. 2a and d, it can be clearly observed that the Co-GSMs synthesized by solvothermal reaction show rather uniform and solid nanosphere morphology with smooth surface and the average particle size is approximately 1 μm. Subsequently, in the hydrothermal process, the glycerate alkoxides hydrolyzed and the morphology transformed from initial solid nature to hierarchical hollow structure. As time went by, the uniform and hierarchical hollow microspheres was eventually constructed by self-assembly of Co_3O_4 nanosheets, which can be explained by the Kirkendal effect. The thickness of Co_3O_4 nanosheets is about 25 nm, shown in Fig. 2b. To display the regulation process, the SEM images under different volume ratio of water/ethanol are shown in Fig. S1 (ESI, Fig. S1†). It is found that the volume ratio of water/ethanol has an important effect on the morphology of the product. When the volume ratios are set as 2 : 1 and 1 : 1 in the hydrothermal etching reaction system, the as-synthesized hollow microspheres are assembled by nanosheets with internal void space. Nevertheless, when the volume ratio of water/ethanol increased, a mass of broken hollow microspheres are generated, which indicated the excessive amount of water is not conducive to maintaining morphology and structure. Note that, after *in situ* vulcanization, surprisingly, the hollow morphology maintained without serious damage (Fig. 2). The detailed hollow structure and element distribution of hierarchical CoS_2 hollow microspheres were corroborated by further observation with TEM and HRTEM images. As observed in Fig. 2f, the CoS_2 microspheres composed of the wrinkled nanosheets displayed obvious hollow structure and distinct interior cavity, which could tremendously enhance the specific surface area, restricting the occurrence of agglomeration.

Further crystalline structural insights and purity of as-obtained products were examined by powder X-ray diffraction (XRD) measurements (Fig. 3). The characteristic broad diffraction peak located at 10.5° did not appear, indicating the amorphous nature of the as-prepared Co-glycerate complex precursor.[19] After hydrothermal etching, there are several diffraction peaks appearing at 19.0°, 31.3°, 36.8°, 44.8°, 59.4°, 65.2° corresponding to the (111), (220), (311), (400), (511) and (440) crystal planes of Co_3O_4 (PDF#43-1003), respectively.[20–22] Moreover, the results confirmed that Co^{2+} coming out of the dissolution of Co-glycerate complex precursor reacted with CO_3^{2-} groups stepped from the decomposition of organic components of glycerinum and OH^- to form the special hierarchical Co-based carbonate hydroxide hollow microspheres. After drying, hierarchical Co-based carbonate hydroxide hollow microspheres turn into Co_3O_4 hollow microspheres. After *in situ*

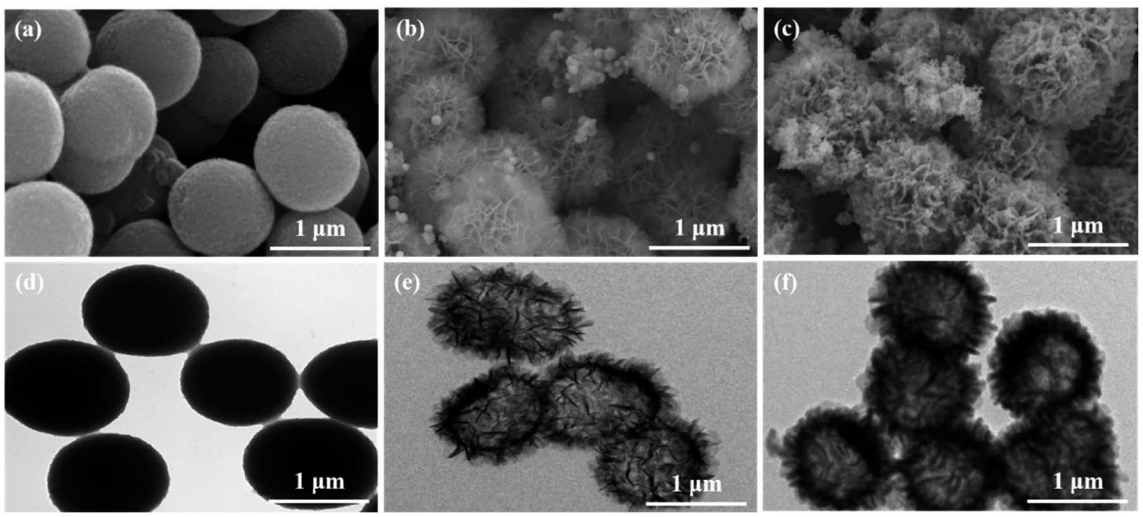

Fig. 2 SEM and TEM images of Co-GSMs (a and d), Co_3O_4 (b and e), hierarchical CoS_2 hollow microspheres (c and f).

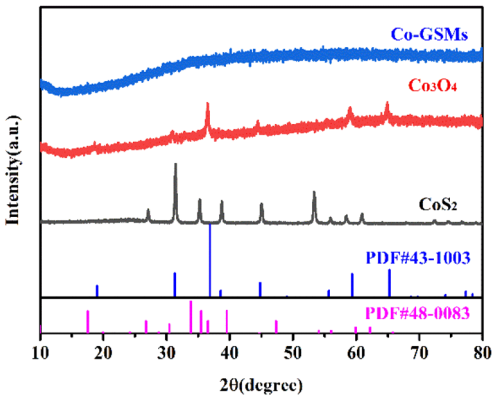

Fig. 3 XRD patterns of the samples Co-GSMs (blue line), Co_3O_4 (red line), CoS_2 (black line).

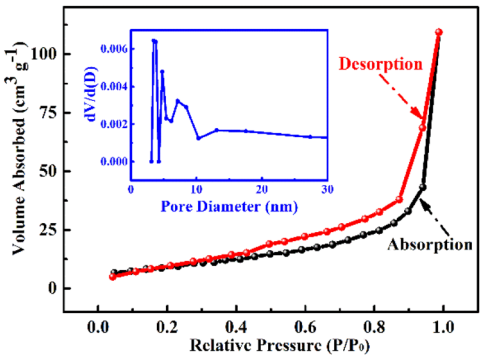

Fig. 5 The N_2 adsorption–desorption isotherm curve and pore diameter distribution of the as-prepared sample.

vulcanization process, XRD curve exhibited certain major diffraction peaks at 27.5°, 32.0°, 36.2°, 39.5°, 46.0°, 54.5°, 57.6°, 60.1° and 62.5°, which could be indexed to the (111), (200), (210), (211), (220), (311), (222), (230) and (321) planes of hierarchical CoS_2 hollow microspheres (PDF#41-1471).[23,24]

The chemical elemental composition and the electronic interaction of the samples were further identified by X-ray photoelectron spectroscopy (XPS). The survey spectrum of Co-glycerate precursor solid microspheres and demonstrated the existence of C, O, and Co elements (Fig. S2†). Compared to Co-GSMs, Co_3O_4 contain the same elemental composition with the slightly different peak intensity. The atomic ratio of C/O/Co obtained from the XPS survey spectra of Co-GSMs and Co-GHMs (ethanol/H_2O = 1 : 1) were calculated to be 11.7 : 4:1 and 4.3 : 3:1, respectively. Moreover, the survey scan spectrum in Fig. S2† verified the successful introduction of S element through the *in situ* vulcanization process, which was consistent with the previous XRD measurements. And the atomic ratio of Co to S is calculated to be 1 : 2.13, similar to the designed ratio. For the high-resolution Co 2p spectrum in Fig. 4a, the prominent characteristic peaks centered at 781.5 eV and 797.7 eV corresponded to the Co $2p_{3/2}$ and Co $2p_{1/2}$, and the peaks at 785.1 eV and 802.7 eV are two shakeup satellites, respectively.[25–27] The corresponding S 2p spectrum (Fig. 4b) displays the deconvoluted peaks at 169.5 eV assigned to S–O bond, and 162.4 eV as well as 163.7 eV, which were ascribed to the S $2p_{3/2}$ and S $2p_{1/2}$ orbitals, respectively.[28–30] Simultaneously, N_2 adsorption–desorption isotherms were performed to further reveal the specific surface area and porous structure. As shown in Fig. 5, the composites showed typical IV-type isothermal curve with a distinct and narrow hysteresis loop. The specific surface area of hierarchical CoS_2 hollow microspheres reached up to 118 $m^2\ g^{-1}$ and the pore size was about 3.54 nm, respectively. Generally speaking, the hierarchical porous structure is not only beneficial to optimize impedance matching, but also to enhance interface polarization and multiple scatterings.[31]

To explore the microwave absorption performance of the as-obtained products, the electromagnetic parameters of various contents samples mixed with paraffin by a simple blending method were measured. The theoretical reflection loss (RL) values of CoS_2/wax composites with different CoS_2 proportions at various thicknesses were estimated by the following eqn (1) and (2) according to the transmission line theory.[32–34]

$$Z_{in} = Z_0\sqrt{\mu_r/\varepsilon_r}\tan h\left(j\frac{2\pi fd}{c}\sqrt{\mu_r/\varepsilon_r}\right) \quad (1)$$

$$RL(dB) = 20\log\left|\frac{Z_{in}-Z_0}{Z_{in}+Z_0}\right| \quad (2)$$

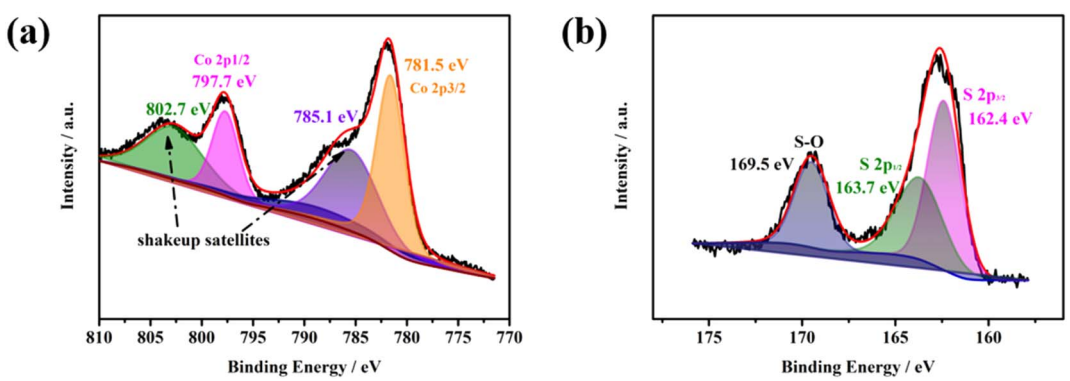

Fig. 4 The high-resolution Co 2p (a) and S 2p (b) spectrum.

where Z_{in}, Z_0, ε_r, μ_r, f, d and c represent the input characteristic impedance, the impedance of the free space, the complex permittivity, the complex permeability, the frequency, the thickness of the absorber and the speed of light, respectively. Fig. 6 show the contours of reflection loss values and 2D curves of the different composites. From RL curves, the microwave absorption performance of all samples show great differences. CS15 samples present terrible microwave absorption performance with the minimum RL value of −11.0 dB and the maximum effective absorption bandwidth (RL < −10 dB) is only 1.1 GHz with the thickness of 4.7 mm. It is worthy noting that when the filling content reached to 25% (CS25), the reflection loss values and the effective absorption bandwidth have become significantly larger and wider than that of CS15 samples (Fig. 6b and e). The effective absorption band (EAB) can be achieved in the frequency range of 5.6–18.0 GHz with the thickness of 1.0–5.0 mm. The minimum RL value of −47.3 dB and the corresponding effective absorption band 8.4 GHz could be obtained as well as the widest 9.0 GHz EAB at a single thickness of only 3.3 mm and 3.2 mm, respectively. For CS35, the EAB can be obtained from 11.5–18.0 GHz with the minimum RL value of −34.2 dB at 14.2 GHz at the thickness of 2.5 mm, which manifest the minimum RL value and the EAB decreased to some extent. The optimal values with different filler loadings are shown in Fig. 6, it can be seen that the maximum EAB of CS25 samples covered 50% of the measured frequency range and covered the whole Ku band and most of the X band. Impressively, the minimum reflection loss values of the hierarchical

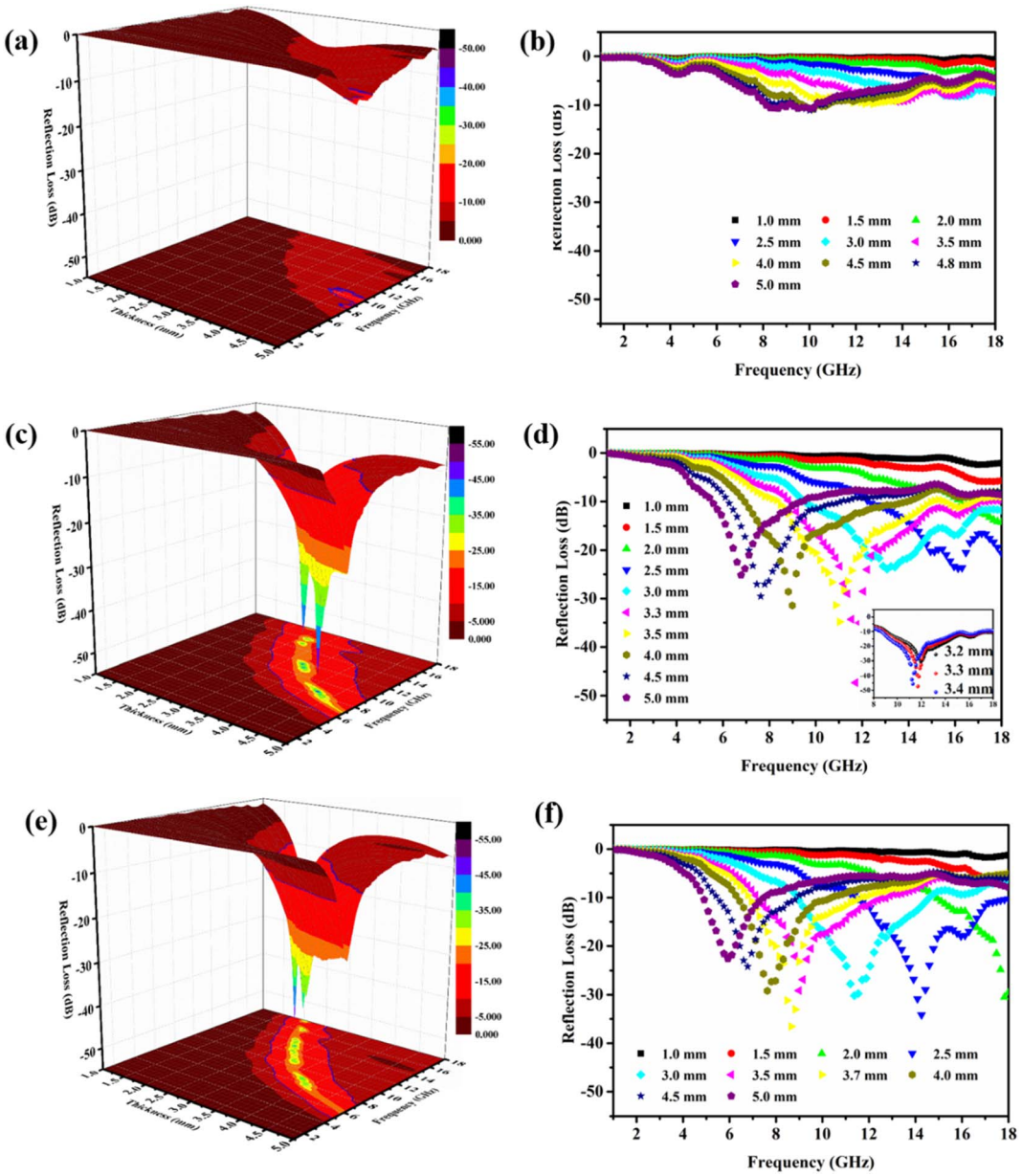

Fig. 6 The contours of reflection loss values and 2D curves of CS15 (a and d), CS25 (b and e), CS35 (c and f) in the frequency range of 1.0–18.0 GHz with increased thickness from 1.0 to 5.0 mm.

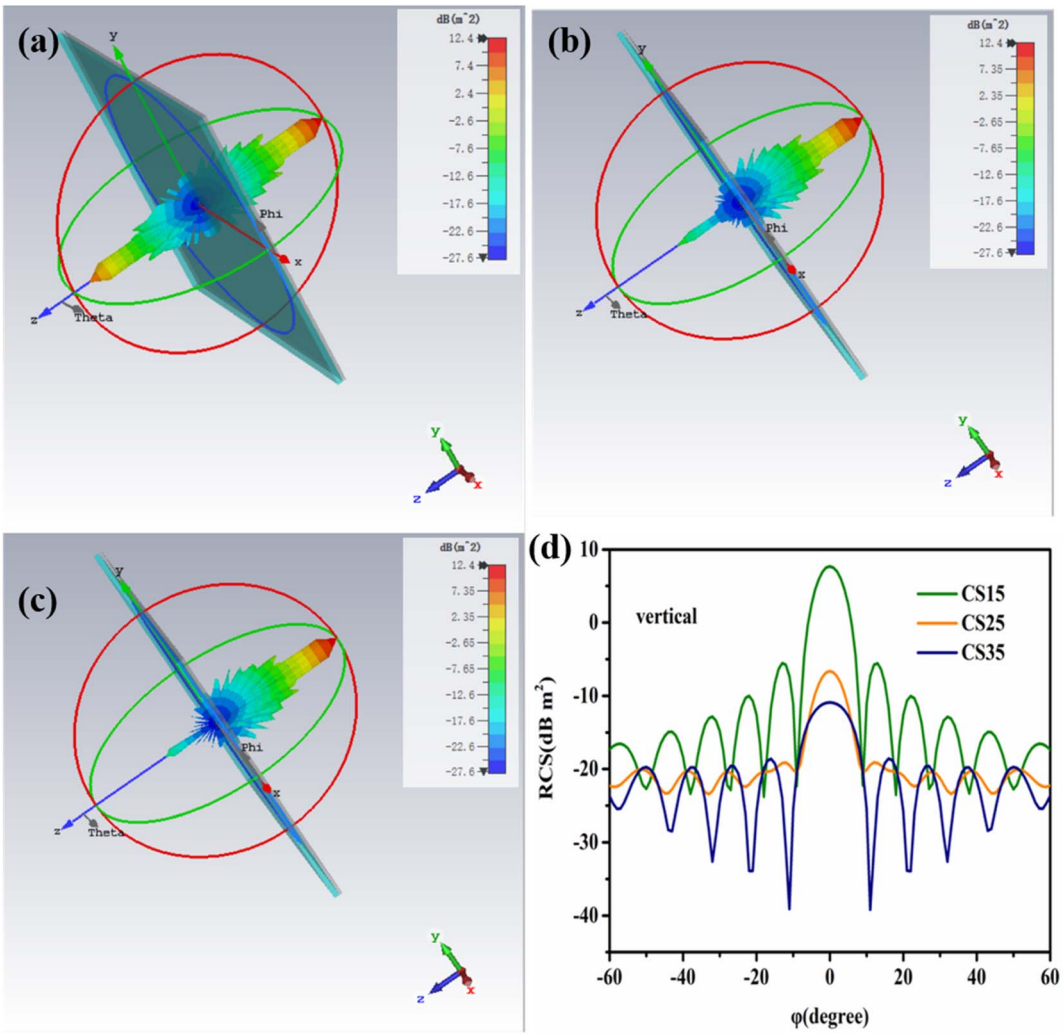

Fig. 7 The 3D RCS values of CS15 (a), CS25 (b), and CS35 (c). (d) The 2D RCS values of CS15, CS25 and CS35 composites in vertical polarization.

CoS_2 hollow microspheres with different filling loadings shift to lower frequency as the thicknesses elevate in the frequency range of 1–18 GHz, which can be explained by the quarter-wavelength matching model (Fig. 6 and Fig. S3†).[35] By comparison, whether peak intensity of the RL values or width of EAB, CS25 samples have advantages over CS15 and CS35 (Fig. 8). To convince the practical stealth performance parameters, the radar cross section (RCS) of different samples were

Table 1 Microwave Absorption Properties of CoS_2-Based Composites

Material	Matrix	Ratio (wt%)	Thickness (mm)	Frequency range (GHz)	RL_{min} (dB)	Ref.
CoS hollow spheres (CHSs)	Wax	20%	2.0	13.2–17.8	−43.6	36
$Co_{1-x}S$ hollow spheres	PVDF	3%	2.5	11.04–16.64	−46.1	37
CuS@CoS_2 nanoboxes	Wax	30%	2.2	9.8–18	−50.1	38
Hollow CuS@CoS_2 nanoboxes	Wax	25%	—	—	−54.9	39
Porous Co_9S_8 nanotubes	Wax	30%	1.5	12.64–17.68	−16.93	40
Porous Co_9S_8 nanotubes	Wax	20%	2.8	8.08–12.08	−46.73	40
CoS_2 hollow nanoboxes	Wax	20%	2.3	12–18	−38.09	41
CoS_2–MoS_2 composites	Wax	—	3.62	2.56	−71.56	42
CC@NPC/CoS_2 composites	Wax	30%	2.8	10.8–18	−59.6	43
CoS_2/rGO	Wax	50%	2.2	9.1–13.2	−56.9	44
CoS_2 hollow microsphere	**Wax**	**25%**	**3.2**	**9–18**	**−30.5**	**This work**
CoS_2 hollow microsphere	**Wax**	**25%**	**3.3**	**9–17.4**	**−47.3**	**This work**

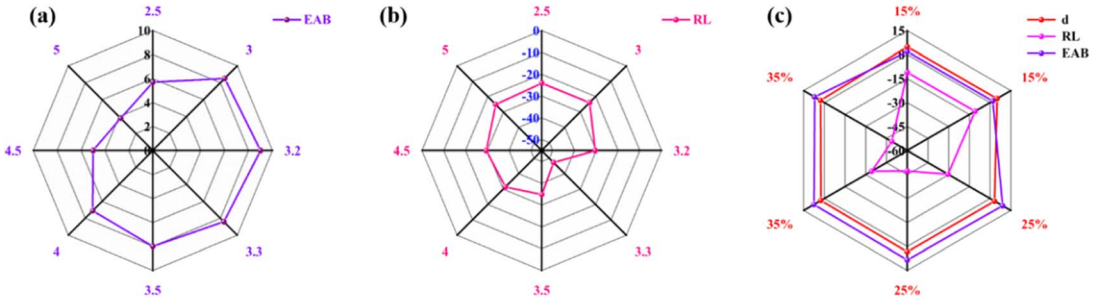

Fig. 8 Various Radar graphs of (a) d-EAB, (b) d-RL and (c) d-RL-EAB at different filling contents.

simulated by the CST microwave studio. The simulation results are shown in the Fig. 7a–d, compared with CS15 sample, the RCS values for CS25 and CS35 could maintain values below −20 dB m^2 at most incident angles ($-60° \leq \varphi \leq 60°$, φ represents the angle of incidence in the simulation model), demonstrating that the CS25 and CS35 show better microwave absorption performance than that of CS15, which is consistent with the previous discussion. A comparison of the microwave absorption performance between the hierarchical CoS_2 hollow microspheres and other reported literature is listed in Table 1. As shown, the hierarchical CoS_2 hollow microspheres display impressive performance compared with other absorbers, in view of splendid absorption intensity and wide bandwidth Fig. 8.

To embody the mechanism of the dielectric loss of CoS_2 in detail, the real and imaginary parts (ε' and ε'') of complex permittivity of different samples are shown in Fig. 9. The real part of permittivity represent the energy storage ability, whereas the imaginary part of permittivity reveal the energy dissipation, respectively.[45–47] Evidently, the ε' and ε'' of complex permittivity show an increase trend with increasing filling contents of CoS_2, indicating the enhanced dielectric loss, which could be explained by the effective medium theory.[48] Synchronously, the ε' and ε'' show a downward trend through vigorous fluctuation occurred at high frequency with the increasing of frequency, which demonstrated the existence of the frequency dispersion effect.[49] For CS25 and CS35, they possess higher ε' and ε'' values than those of CS15, indicating a greater capacity to store electrical energy and a more outstanding dielectric loss (Fig. 9a and b). Remarkably, steady ε' values are beneficial to suitable impedance matching, so the several obvious plateaus at 15 GHz and 17 GHz of ε' curve of all samples will do harm to impedance matching properties.

According to the Debye theory and free electron theory, it is deduced that dipolar polarization triggered by the defects in materials, interfacial polarization originating by various interfaces and transition metal sulfides materials inherent conductivity loss together give rise to dielectric loss. Based on the above points, CS25 and CS35 samples deliver the stronger dielectric loss as shown in Fig. 9c, and the dielectric loss values maintain a general upward trend. By virtue of the local symmetry breaking of the hierarchical CoS_2 hollow microspheres surface atoms, the enhanced dipole polarization is introduced and the corresponding relaxation process is of pivotal importance to augment the microwave absorption performance, which can be verified by the Cole–Cole semicircle. According to the Debye dipolar relaxation, the relative complex permittivity (ε_r) can be estimated by the following equation:[50]

$$\varepsilon_r = \varepsilon' - j\varepsilon'' = \varepsilon_\infty + \frac{\varepsilon_s - \varepsilon_\infty}{1 + j2\pi f\tau} \quad (3)$$

in which ε_s, τ and ε_∞ represent the static permittivity, the polarization relaxation time, and relative dielectric permittivity at the high-frequency limit, respectively. From eqn (3), it can be deduced as shown below

$$\varepsilon' = \varepsilon_\infty + \frac{\varepsilon_s - \varepsilon_\infty}{1 + (2\pi f)2\tau 2} \quad (4)$$

$$\varepsilon'' = \frac{2\pi f\tau(\varepsilon_s - \varepsilon_\infty)}{1 + (2\pi f)2\tau 2} \quad (5)$$

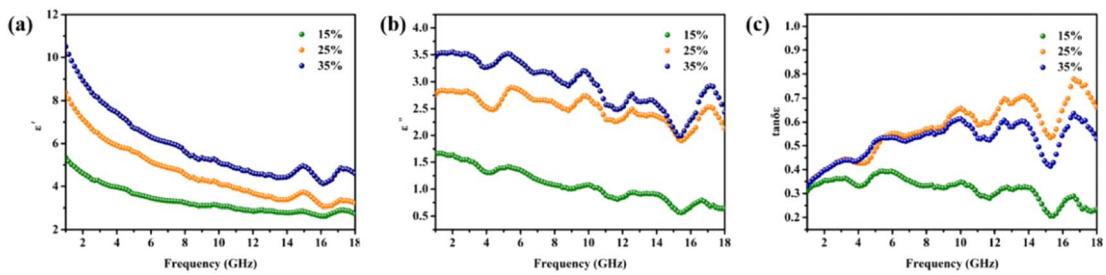

Fig. 9 Frequency dependence of the real and imaginary parts of complex permittivity (a) and (b), dielectric loss tangent (c) of CS15, CS25 and CS35.

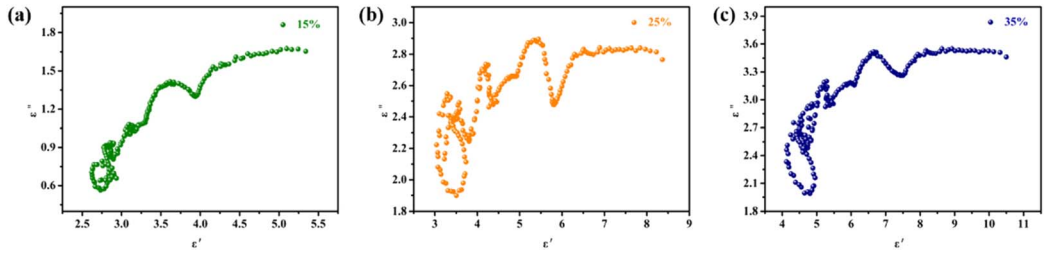

Fig. 10 The Cole–Cole plots of (a) CS15, (b) CS25 and (c) CS35 samples.

According to eqn (4) and (5), the final relationship between ε' and ε'' can be deduced as:[31,51]

$$\left(\varepsilon' - \frac{\varepsilon_s + \varepsilon_\infty}{2}\right)2 + (\varepsilon'')2 = \left(\frac{\varepsilon_s - \varepsilon_\infty}{2}\right)2 \quad (6)$$

Apparently, the ε' *versus* ε'' curve would perform a single semicircle, which commonly was referred to Cole–Cole semicircle, and one relaxation process usually corresponds to one semicircle. As shown in Fig. 10, there is more than one semicircle suggesting the multiple Debye relaxation process in all samples. Besides, the Cole–Cole semicircles of CS25 and CS35 samples show similar changes. But without ignorance, the Cole–Cole semicircles are distorted, indicating there are might some other mechanisms, such as the Maxwell–Wagner relaxation.[52] Additionally, as depicted in Fig. 10, there is a long and straight line in the Cole–Cole curve of all samples at low frequency, which indicated that the conduction loss has certain contributions to the enhanced microwave absorption performance.

The impedance matching (Z) is an important parameter to be considered in achieving superior absorption performance, which can be derived from the following formula:[47]

$$Z = Z_{in}/Z_0 = \sqrt{\mu_r/\varepsilon_r}\tan h\left(j\frac{2\pi fd}{c}\sqrt{\mu_r\varepsilon_r}\right) \quad (7)$$

As we all know, when the impedance matching Z value is close to 1, the electromagnetic wave tends to go into the material rather than being reflected at the interface.[53] As shown in Fig. 11, the light green area between $Z = 0.75$ and $Z = 1.5$ is enclosed in blue. Admittedly, the bigger the enclosed area is, the better the impedance matching Z value is. Obviously, it can be seen that the CS15 and CS25 have better impedance matching, and the impedance matching Z values of CS35 are still far from satisfactory due to the high filling contents (Fig. 11).

The attenuation coefficient (α) of the microwave absorbers represents the dissipation characteristics and capacity of the absorbing materials, which is mainly dominantly by the relative complex permittivity and the relative complex permeability. The attenuation coefficient α could be expressed by the following equation:[54,55]

$$\alpha = \frac{\sqrt{2}\pi f}{c}\sqrt{(\mu''\varepsilon'' - \mu'\varepsilon') + \sqrt{(\mu''\varepsilon'' - \mu'\varepsilon')^2 + (\mu'\varepsilon'' + \mu''\varepsilon')^2}} \quad (8)$$

Apparently, as shown in Fig. 12, the attenuation coefficient α maintained a continuous upward trend with the increase of

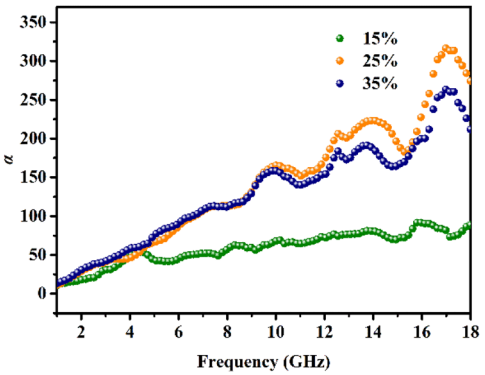

Fig. 12 Characteristic attenuation coefficient α of samples.

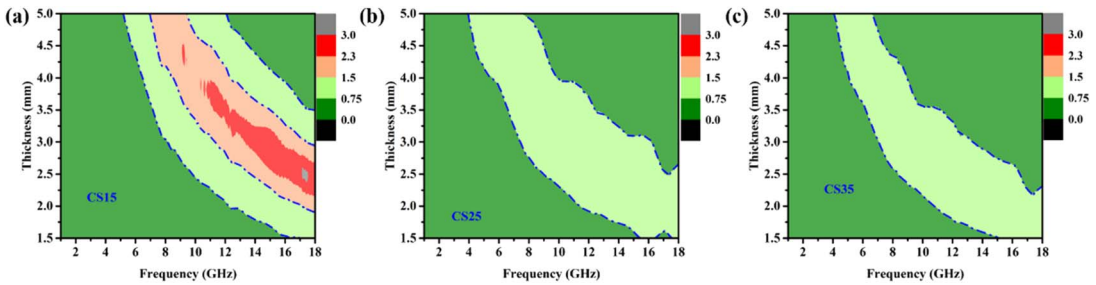

Fig. 11 Characteristic impedance matching Z of samples (a) CS15, (b) CS25 and (c) CS35.

the frequency. The attenuation coefficient (α) values of CS15 is much lower than that of CS25 and CS35, leading to the weak EW attenuation ability. Impressively, CS25 samples possess multiple advantages in terms of the impedance matching (Z) values and attenuation coefficient (α). According to the above results, CS25 have better impedance matching and higher attenuation coefficient α, which resulted in the enhanced microwave absorption performance.

Based on the above considerations, the associated microwave absorption mechanism of the hierarchical CoS_2 hollow microspheres mainly come from the following aspects. Initially, the dipoles polarization and defect polarization because of the existing defects in hollow structure as well as the multiple interfacial polarizations originated from the abundant interfaces and multiple cores which can act as polarized centers and induce the associated resonance relaxation processes further enhance the dielectric loss. Afterward, multiple scattering and reflection stemming from the hierarchical hollow structure increase the propagation path of the incident electromagnetic wave, thus contributing to enhancing microwave absorption. Finally, the optimal balance between impedance matching and attenuation ability make microwave entry into the absorbents and favor the microwave attenuate.

Conclusion

In summary, the hierarchical dandelion-like CoS_2 hollow microspheres have been rationally designed and successfully prepared by multiple steps including solvothermal reaction and hydrothermal etching as well as subsequent *in situ* vulcanization process. Notably, the morphology and structure of the products can be easily adjusted by controlling the volume ratio of ethanol/H_2O, which dominated the electromagnetic wave absorption properties. More specifically, benefiting from the outstanding structural advantages and the coexistence of dielectric loss and magnetic loss as well as the synergetic effect for CoS_2 hollow microspheres, it is found that the optimized CoS_2/paraffin composites exhibit the significantly enhanced electromagnetic wave absorption properties with the qualified frequency bandwidth of up to 9.0 GHz (namely broad effective absorption bandwidth 9.0–18.0 GHz; RL ≤ -10 dB) and the minimum reflection loss value (-47.3 dB) at a thin thickness of only 3.3 mm. These results demonstrate that the hierarchical CoS_2 hollow microspheres could be attractive candidate materials for MAMs with wider absorption frequency bandwidth and smaller filler loading.

Conflicts of interest

There are no conflicts to declare.

Acknowledgements

The work was supported by the grants from Natural Science Foundation of Henan Province (No.232300420332), the Key Scientific Research Project of Higher Education Institutions in Henan Province (23A430006), the Youth Research Funds Plan of Zhengzhou University of Aeronautics (23ZHQN01005), the National Natural Science Foundation of China (No. 51873109), the Liaoning Revitalization Talents Program (No. XLYC1802085) and Dalian Science and Technology Innovation Fund Project (2019J11CY007).

References

1 C. P. Li, D. Li, L. Zhang, Y. H. Zhang, L. Zhang, C. H. Gong and J. W. Zhang, Boosted microwave absorption performance of transition metal doped TiN fibers at elevated temperature[J], *Nano Res.*, 2023, **16**, 3570–3579.
2 Z. N. Xiang, B. K. Xu, Q. C. He, Y. Q. Wang and X. M. Yin, Synergistic magnetic/dielectric loss of Fe_3Si/SiC composites for efficient electromagnetic wave absorption[J], *Chem. Eng. J.*, 2023, **457**, 141198.
3 G. R. Yang, B. Wen, Z. Y. Zhou, S. L. Wang, H. Y. Zhao, S. J. Ding and W. Yan, Flexible cobalt nanoparticles/carbon nanofibers with macroporous structures toward superior electromagnetic wave absorption[J], *J. Colloid Interface Sci.*, 2023, **636**, 194–203.
4 C. H. Sun, Z. R. Jia, S. Xu, D. Q. Hu, C. H. Zhang and G. L. Wu, Synergistic regulation of dielectric-magnetic dual-loss and triple heterointerface polarization *via* magnetic MXene for high-performance electromagnetic wave absorption[J], *J. Mater. Sci. Technol.*, 2022, **113**, 128–137.
5 Z. H. Zhao, D. Lan, L. M. Zhang and H. J. Wu, A flexible, mechanically strong, and anti-corrosion electromagnetic wave absorption composite film with periodic electroconductive patterns[J], *Adv. Funct. Mater.*, 2022, **32**, 2111045.
6 S. K. Hou, Y. Wang, F. Gao, F. Y. Wang, H. Yang, F. Jin, G. X. Bai, Z. H. Cao and Y. C. Du, In situ growing fusiform SnO_2 nanocrystals film on carbon fiber cloth as an efficient and flexible microwave absorber[J], *Mater. Des.*, 2023, **225**, 111576.
7 S. B. Cao, H. B. Liu, L. Yang, Y. H. Zou, X. H. Xia and H. Chen, The effect of microstructure of graphene foam on microwave absorption properties[J], *J. Magn. Magn. Mater.*, 2018, **458**, 217–224.
8 X. Ling, K. F. Wang, W. Zhang, Y. Wu, Q. J. Jin and D. Zhang, Bio-inspired, bimetal ZIF-derived hollow carbon/MXene microstructure aim for superior microwave absorption[J], *J. Colloid Interface Sci.*, 2022, **625**, 317–327.
9 X. Y. Yuan, W. R. Huang, X. M. Zhang, J. Z. Wang, Y. Liu, L. Kong and S. W. Guo, Carbon-coated Mn_4N nanowires with abundant internal voids for microwave absorption[J], *ACS Appl. Nano Mater.*, 2019, **2**, 7848–7855.
10 J. L. Pan, R. J. Zhang, Z. Zhen, M. Wang, Z. C. Li, D. F. Yin, L. Y. Meng, L. M. He and H. W. Zhu, Enhanced microwave absorption of shape anisotropic Fe_3O_4 nanoflakes and their composites[J], *Adv. Eng. Mater.*, 2022, **24**, 2100790.
11 X. X. Wang, K. Fu, X. Y. Wen, S. C. Qi, G. X. Tong, X. J. Wang and W. H. Wu, Oxygen vacancy boosted microwave absorption in CeO_2 hollow nanospheres[J], *Appl. Surf. Sci.*, 2022, **598**, 153826.

12 H. Q. Zhao, Y. Cheng, W. Liu, L. J. Yang, B. S. Zhang, L. P. Wang, G. B. Ji and Z. J. Xu, Biomass-derived porous carbon-based nanostructures for microwave absorption[J], *Nano-Micro Lett.*, 2019, **11**, 24.

13 M. X. Sun, W. Q. Cao, P. Y. Zhu, Z. M. Xiong, C. C. Chen, J. C. Shu, W. H. Huang and F. Wu, Thermally tailoring magnetic molecular sponges through self-propagating combustion to tune magnetic-dielectric synergy toward high-efficiency microwave absorption and attenuation[J], *Adv. Compos. Hybrid Mater.*, 2023, **6**, 54.

14 X. L. Cao, X. H. Liu, J. H. Zhu, Z. R. Jia, J. K. Liu and G. L. Wu, Optimal particle distribution induced interfacial polarization in hollow double-shell composites for electromagnetic waves absorption performance[J], *J. Colloid Interface Sci.*, 2023, **634**, 268–278.

15 H. X. Zhang, K. G. Sun, K. K. Sun, L. Chen and G. L. Wu, Core-shell Ni_3Sn_2@C particles anchored on 3D N-dope d porous carbon skeleton for modulated electromagnetic wave absorption[J], *J. Mater. Sci. Technol.*, 2023, **158**, 242–252.

16 X. K. Wang, C. Hao, J. S. Zhang, C. H. Ni, X. H. Wang and Y. T. Shen, Reasonable design and synthesis of nickel manganese sulfide nanoparticles derived from metal organic frameworks as electrode materials for supercapacitors[J], *J. Power Sources*, 2022, **539**, 231594.

17 D. Kim, J. G. Song, H. Yang, H. Y. Lee, J. Park and H. J. Kim, Textile-based high-performance hydrogen evolution of low-temperature atomic layer deposition of cobalt sulfide[J], *Nanoscale*, 2019, **11**, 844–850.

18 S. Khan, H. Choi, D. H. Kim, S. Y. Lee, Q. H. Zhu, J. L. Zhang, S. C. Kim and S. H. Cho, Self-assembled heterojunction of metal sulfides for improved photocatalysis[J], *Chem. Eng. J.*, 2020, **395**, 125092.

19 Y. Lu, J. W. Nai and X. W. David Lou, Formation of $NiCo_2V_2O_8$ yolk-double shell spheres with enhanced Lithium storage properties[J], *Angew. Chem., Int. Ed.*, 2018, **57**, 2899–2903.

20 B. Y. Guan, L. Yu, X. Wang, S. Y. Song and X. W. (David) Lou, Formation of onion-like $NiCo_2S_4$ particles *via* sequential ion-exchange for hybrid supercapacitors[J], *Adv. Mater.*, 2017, **29**, 1605051.

21 W. Du, R. M. Liu, Y. W. Jiang, Q. Y. Lu, Y. Z. Fan and F. Gao, Facile synthesis of hollow Co_3O_4 boxes for high capacity supercapacitor[J], *J. Power Sources*, 2013, **227**, 101–105.

22 X. J. Lian, W. Guo, Y. L. Wu, Y. M. Tian and S. Wang, The structure-stabilized Co_3O_4@Co_9S_8 core-shell nanorods synthesized by in-situ sulfuration of Co_3O_4 for high-performance supercapacitors[J], *J. Alloys Compd.*, 2021, **865**, 158296.

23 Z. P. Zhao, S. H. Li, C. Q. Li, Z. Y. Liu and D. Li, Hollow CoS_2@C nanocubes for high-performance sodium storage [J], *Appl. Surf. Sci.*, 2020, **519**, 146268.

24 Y. P. Hua, H. Jiang, H. B. Jiang, H. X. Zhang and C. Z. Li, Hierarchical porous CoS_2 microboxes for efficient oxygen evolution reaction[J], *Electrochim. Acta*, 2018, **278**, 219–225.

25 X. P. Liu, S. F. Deng, D. D. Xiao, M. X. Gong, J. N. Liang, T. H. Zhao, T. Shen and D. L. Wang, Hierarchical bimetallic Ni-Co-P microflowers with ultrathin nanosheet arrays for efficient hydrogen evolution reaction over all pH values[J], *ACS Appl. Mater. Interfaces*, 2019, **11**, 42233–42242.

26 L. S. Shen, H. W. Song, G. Z. Yang and C. X. Wang, Hollow ball-in-ball $Co_xFe_{3-x}O_4$ nanostructures: high-performance anode materials for lithium-ion battery[J], *ACS Appl. Mater. Interfaces*, 2015, **7**, 11063–11068.

27 L. R. Hou, R. Q. Bao, M. Rehan, L. N. Tong, G. Pang, X. G. Zhang and C. Z. Yuan, Uniform hollow mesoporous nickel cobalt sulffde microdumbbells: a competitive electrode with exceptional gravimetric/volumetric pseudocapacitance for high-energy-density hybrid superapacitors[J], *Adv. Bioelectron. Mater.*, 2017, 1600322.

28 X. L. Chen, C. Liu, C. K. Tang, Z. H. Liu, Q. F. Lü and Y. Q. Jin, CoS_2 nanoparticles grown on Mo2TiC2Tx as an efffcient electrocatalyst for hydrogen evolution reaction[J], *Diamond Relat. Mater.*, 2023, **135**, 109877.

29 J. Xu, P. Ye, Y. W. Cheng, L. Ji, Y. C. Wei and Y. P. Chen, Metal-organic framework-based CoS_2 nitrogen-doped carbon for high-performance lithium storage[J], *Energy Technol.*, 2023, **11**, 2201452.

30 T. Q. Hou, J. W. Wang, T. T. Zheng, Y. Liu, G. L. Wu and P. F. Yin, Anion exchange of metal particles on carbon-based skeletons for promoting dielectric equilibrium and high-efficiency electromagnetic wave absorption[J], *Small*, 2023, 2303463.

31 H. Y. Wang, X. B. Sun, Y. Xin, S. H. Yang, P. F. Hu and G. S. Wang, Ultrathin self-assembly MXene/Co-based bimetallic oxide heterostructures as superior and modulated microwave absorber[J], *J. Mater. Sci. Technol.*, 2023, **134**, 132–141.

32 X. L. Li, X. W. Yin, C. Q. Song, M. K. Han, H. L. Xu, W. Y. Duan, L. F. Cheng and L. T. Zhang, Self-assembly core-shell graphene-bridged hollow MXenes spheres 3D foam with ultrahigh speciffc EM absorption performance [J], *Adv. Funct. Mater.*, 2018, 1803938.

33 C. H. Wang, L. S. Zong, Y. X. Pan, N. Li, Q. Liu, J. Y. Wang and X. G. Jian, Preparation and characterization of branch-like heteroatoms-doped Ni@C nanoffbers for high-performance microwave absorption with thin thickness[J], *Composites, Part B*, 2021, **223**, 109114.

34 W. X. Min, D. W. Xu, P. Chen, G. Z. Chen, Q. Yu, H. F. Qiu and X. Y. Zhu, Synthesis of novel hierarchical CoNi@NC hollow microspheres with enhanced microwave absorption performance[J], *J. Mater. Sci.: Mater. Electron.*, 2021, **32**, 8000–8016.

35 X. J. Zeng, X. Y. Cheng, R. H. Yu and G. D. Stucky, Electromagnetic microwave absorption theory and recent achievements in microwave absorbers[J], *Carbon*, 2020, **168**, 606–623.

36 T. Y. Huang, M. He, Y. M. Zhou, S. W. Li, B. B. Ding, W. L. Pan, S. Huang and Y. Tong, Solvothermal synthesis of flower-like CoS hollow microspheres with excellent microwave absorption properties[J], *RSC Adv.*, 2016, **6**, 100392.

37 X. J. Zhang, J. Q. Zhu, P. G. Yin, A. P. Guo, A. P. Huang, L. Guo and G. S. Wang, Tunable high-performance microwave

absorption of $Co_{1-x}S$ hollow spheres constructed by nanosheets within ultralow filler loading[J], *Adv. Funct. Mater.*, 2018, 1800761.

38 P. B. Liu, S. Gao, X. D. Liu, Y. Huang, W. J. He and Y. T. Li, Rational construction of hierarchical hollow CuS@CoS_2 nanoboxes with heterogeneous interfaces for high-efficiency microwave absorption materials[J], *Composites, Part B*, 2020, **192**, 107992.

39 F. Z. Zeng, L. Li, C. Y. Liu and Z. Lin, Hollow CoS_2 nanobubble prisms derived from ZIF-67 through facile two-step self-engaged method for electromagnetic wave absorption[J], *ChemistrySelect*, 2021, **6**, 4344–4353.

40 C. H. Zhou, C. Wu, H. P. Lv and M. Y. Porous, Co_9S_8 nanotubes with the percolation effect for lightweight and highly efficient electromagnetic wave absorption[J], *J. Mater. Chem. C*, 2019, **7**, 1696–1704.

41 D. W. Xu, H. H. Guo, F. F. Zhang, Y. M. Wu, X. Q. Guo, Y. M. Ren and D. F. Feng, In situ formation of CoS_2 hollow nanoboxes *via* ion-exchange for high-performance microwave absorption[J], *Nanomaterials*, 2022, **12**, 2876.

42 J. L. Ma, H. D. Ren, X. M. Zhang, Z. Y. Liu, S. Wang, W. Lian, C. Li, Y. Liu and L. B. Kong, Multilayer rose-like CoS_2-MoS_2 composites with high microwave absorption performance [J], *J. Magn. Magn. Mater.*, 2023, **568**, 170390.

43 P. B. Liu, C. Y. Zhu, S. Gao, C. Guan, Y. Huang and W. J. He, N-doped porous carbon nanoplates embedded with CoS_2 vertically anchored on carbon cloths for flexible and ultrahigh microwave absorption[J], *Carbon*, 2020, **163**, 348–359.

44 C. Zhang, B. C. Wang, J. Y. Xiang, C. Su, C. P. Mu, F. S. Wen and Z. Y. Liu, Microwave absorption properties of CoS_2 nanocrystals embedded into reduced graphene oxide[J], *ACS Appl. Mater. Interfaces*, 2017, **9**, 28868–28875.

45 W. J. Yu and G. F. Shao, Morphology engineering of defective graphene for microwave absorption[J], *J. Colloid Interface Sci.*, 2023, **640**, 680–687.

46 P. Y. Zhao, H. Y. Wang, B. Cai, X. B. Sun, Z. L. Hou, J. T. Wu, M. Bai and G. S. Wang, Electrospinning fabrication and ultra-wideband electromagnetic wave absorption properties of CeO_2/N-doped carbon nanofibers[J], *Nano Res.*, 2022, **15**, 7788–7796.

47 J. X. Zhou, Z. R. Jia, Y. Zhang and G. L. Wu, Construction of 3D conductive network by flower-like V_2O_3 synergy with magnetic NiCo for superior electromagnetic wave absorption performance[J], *Mater. Today Phys.*, 2022, **29**, 100902.

48 H. Y. Wang, X. B. Sun and G. S. Wang, A MXene-modulated 3D crosslinking network of hierarchical flower-like MOF derivatives towards ultra-efficient microwave absorption properties[J], *J. Mater. Chem. A*, 2021, **9**, 24571–24581.

49 C. Chen, J. B. Xi, E. Z. Zhou, L. Peng, Z. C. Chen and C. Gao, Porous graphene microflowers for high-performance microwave absorption[J], *Nano-Micro Lett.*, 2018, **10**, 26.

50 B. Wei, C. Y. Zhou, Z. J. Yao, L. L. Xu, Z. J. Li, L. Wan, J. S. Hou and J. T. Zhou, Lightweight and high-efficiency microwave absorption of reduced graphene oxide loaded with irregular magnetic quantum dots[J], *J. Alloys Compd.*, 2021, **886**, 161330.

51 Y. Qiu, Y. Lin, H. B. Yang, L. Wang, M. Q. Wang and B. Wen, Hollow Ni/C microspheres derived from Ni-metal organic framework for electromagnetic wave absorption[J], *Chem. Eng. J.*, 2020, **383**, 123207.

52 C. H. Wang, L. S. Zong, N. Li, Y. X. Pan, Q. Liu, F. F. Zhang, L. Y. Qiao, J. Y. Wang and X. G. Jian, Light-weight 1D heteroatoms-doped Fe_3C@C nanoffbers for microwave absorption with a thinner matching thickness[J], *J. Alloys Compd.*, 2021, **885**, 160968.

53 J. Q. Wang, L. Liu, S. L. Jiao, K. J. Ma, J. N. Lv and J. J. Yang, Hierarchical carbon fiber@MXene@MoS_2 core-sheath synergistic microstructure for tunable and efficient microwave absorption[J], *Adv. Funct. Mater.*, 2020, 2002595.

54 Y. L. Wang, G. S. Wang, X. J. Zhang and C. Gao, Porous carbon polyhedrons coupled with bimetallic CoNi alloys for frequency selective wave absorption at ultralow filler loading[J], *J. Mater. Sci. Technol.*, 2022, **103**, 34–41.

55 L. F. Sun, Q. Q. Zhu, Z. R. Jia, Z. Q. Guo, W. R. Zhao and G. L. Wu, CrN attached multi-component carbon nanotube composites with superior electromagnetic wave absorption performance[J], *Carbon*, 2023, **208**, 1–9.